Computational modelling of the crushing behaviour of pultruded glass-fibre reinforced polymer stub columns

João Alfredo de Lazzari[1], José Almeida Gonilha[1], Nuno Silvestre[2], João Ramôa Correia[1]

[1]*CERIS, Instituto Superior Técnico, University of Lisbon*
Av. Rovisco Pais 1, 1049-001 Lisboa, Portugal
joao.lazzari@tecnico.ulisboa.pt, jose.gonilha@tecnico.ulisboa.pt, joao.ramoa.correia@tecnico.ulisboa.pt
[2]*IDMEC, Instituto Superior Técnico, University of Lisbon*
Av. Rovisco Pais 1, 1049-001 Lisboa, Portugal
nsilvestre@tecnico.ulisboa.pt

Abstract. The popularity of pultruded glass-fibre reinforced polymer (pGFRP) profiles in construction stems from their lightness, strength, and durability. However, gaps remain in understanding their mechanics, notably the "true" material crushing failure. Current methodologies to estimate the compressive resistance of pGFRP profiles rely on small-scale tests on coupons, but there is evidence that the full-section compressive strength diverges considerably from that estimated from laminate testing. This study addresses that gap, investigating the crushing behaviour of pGFRP I-section profiles. To that end, computational models were developed, considering second-order effects due to imperfections and displacements. The model includes Gonilha's damage initiation and progression criteria and also end surface irregularities. The study investigates the amplification of the end surface imperfection compared to a perfect flat end surface, providing insights into stress and deformations resulting from those geometrical defects, envisioning the enhancement of design guidelines for safer and more reliable pGFRP structures.

Keywords: pultruded GFRP profiles; crushing; material damage; composite design guidelines; nonlinear finite element method.

1 Introduction

In recent decades, the use of pultruded glass-fibre reinforced polymer (pGFRP) I-section profiles has gained substantial traction in the construction industry. These profiles are increasingly recognized as a viable choice for building lightweight structures, offering remarkable strength and durability. Nevertheless, due to the relatively recent integration of these profiles in structural applications, there are still significant gaps in our understanding of their mechanical behaviour and geometric attributes. One of these gaps is the absence of a robust definition for the "true" material crushing failure.

Several design guidelines have been established for pGFRP profiles [1]–[5]. However, a consensus regarding the most suitable design and safety assessment procedures has not yet been reached. In the context of axial compressive members, the prevailing approach endorsed by most guidelines is known to be inaccurate – it represents the minimum between resistance to pure material failure and the pure buckling phenomenon, where the compressive material strength is based on results of small-scale coupon (SSC) tests. Moreover, increased uncertainty arises when considering factors like (i) the interaction between material strength and elastic buckling, (ii) the coupling between different buckling modes, and (iii) the influence of initial geometric imperfections.

Traditionally, the crushing resistance of pGFRP profiles is estimated by extrapolating the material's compressive resistance obtained from standardized coupon tests. These tests are conducted on laminates extracted from the walls of the cross-section (according to procedures such as those defined in ASTM D6641-14 [6] and EN 14126 [7]). Nonetheless, recent experimental investigations show that such approach leads to a significant overestimation of the actual crushing resistance of full-section (FS) pultruded profiles, particular for stub columns[8]–[11].

Turvey and Zhang [12], [13] highlighted disparities in the predictions of axial compression resistance derived from coupon tests and comprehensive FS test results. They also identified lower shear and tensile strengths at the web-

flange junction compared to the central regions of the webs and flanges. Additionally, they underscored that defects are more likely to occur in FS specimens in comparison to SSC specimens. Similarly, Ramos [8] identified four potential factors contributing to the lower resistance to material crushing observed in FS compression tests compared to coupon tests: (i) mechanical property heterogeneity across the cross-section, particularly at the web-flange junctions, (ii) variations in compressive strength from different testing standards, (iii) a higher probability of defects in FS tests ("size effects"), and (iv) the influence of surface end defects (such as lack of flatness) in FS compression specimens.

Recently, Wu *et al.* [9] conducted tests on pGFRP channel columns with length ranging from 100 mm to 1400 mm. They reported significantly lower strength of stub columns measuring 100 mm and 200 mm in length, than the corresponding resistance estimates. They attributed this to (i) irregularities in the cross-section shape, leading to non-uniform stress distribution, (ii) non-uniform fibre distribution resulting from the pultrusion process and material imperfections, and (iii) local crushing stemming from stress concentrations or material imperfections, which interact with the local buckling phenomenon of the flange or web.

The authors' prior work [10], [11] evaluated the stress-strain behaviour and the effects of slenderness in the compressive behaviour of pGFRP stub columns. Four cross-section geometries were analysed, and the resistance estimated from tests on standardized coupons was compared with FS experiments. Results were in line with past findings, with FS resistances around 50%~60% of the coupon-predicted resistance; these differences were attributed to factors like (i) profile (mis)alignment, (ii) material variation, and (iii) uneven surface flatness (despite careful preparation of specimens). It was concluded that "pure" material crushing (*i.e.*, without buckling interaction) is achievable for normalized slenderness values lower than 0.7.

Given the numerous uncertainties in assessing pure crushing failure in pGFRP profiles, computational modelling can offer valuable insights into the underlying physical-mechanical behaviour associated to this complex phenomenon. This study, therefore, delves into the computational analysis of the crushing failure of pGFRP I-sections, with a particular focus on evaluating the impact of cut end surface defects, using geometric and physical nonlinear analysis, including a damage initiation and propagation model proposed by Gonilha *et al.* [14]. The imperfections of the end surfaces were object of precise measurements [15], the results of which were integrated into finite element (FE) models, developed with software ABAQUS [16]. The analysis included the amplification of the flatness imperfections, to discern any stress concentration effects on the strength of these intricate, orthotropic, and brittle materials.

2 Overview of experimental data

A pGFRP I-section produced by Creative Composites Group [17] is used for the present study. The pultruded profile is composed of E-glass fibres and polyester resin, features nominal dimensions of 152.4 mm height, 76.2 mm width, and 6.35 mm wall thickness. Mechanical properties were derived from tests on SSCs extracted from the profile's walls (web and flange zones), carried out by Almeida-Fernandes *et al.* [18] and Ramos [8], while the FS test results were taken from previous investigations by Lazzari *et al.* [11] and Ramos [8]. Table 1 presents average and standard deviation values of mechanical properties in compression, tension, and in-plane shear, where *x* represents the longitudinal (pultrusion) direction, *y* the transverse (in-plane) direction, *c* stands for compression, *t* stands for tension and *n* is the number of test replicates.

The experimental measurements of the end cut surface of the I-section profile hold significant importance in this research. As previously mentioned, one of the primary objectives of this paper is to assess the impact of irregularities at the end cut surfaces of pGFRP profiles under axial compression loading. Figure 1 illustrates the measured end cut surface imperfections, made on a stub-column specimen. The stub column specimens were produced by transversely cutting a 6-meter-long profile to a length of 64 mm. The cutting process was carried out using a saw blade machine, followed by a smoothing technique to reduce imperfections resulting from the cutting process. The imperfection measurements were carried out with the aid of a 3D coordinate measurement machine, with an accuracy of 0.01 mm. This approach aligns closely with the measurement procedure outlined in Lazzari *et al.* [15].

As depicted in Figure 1, the amplitude of the end surface imperfections for both bottom and top planes of the I-section profile are minimal, with an error in parallelism of 0.093 mm, a parallelism in degrees of 0.038º, and the flatness of each end surface measuring 0.035 mm and 0.058 mm, respectively.

3 Description of the damage model

Commonly used failure initiation models, such as Tsai-Hill [19], Tsai-Wu [20], and Hashin [21], are favoured for their relative simplicity. These models find broad application in computational analysis and are integrated into commercial FE software like ABAQUS [16]. The damage initiation and propagation model featured in that commercial software was devised by Lapczyk and Hurtado [22], based on the models proposed by Hashin [21], Matzenmiller *et al.* [23], and Camanho and Dávila [24]. However, its usability is confined to shell element formulations due to its formulation and transverse isotropic assumption. To model more complex phenomena, including through-thickness damage, cohesive failure laws must be added to those models to replicate failure between plies.

This study adopts a failure initiation and damage propagation model proposed by Gonilha *et al.* [14], recently calibrated and validated by Costa *et al.* [25]. The model allows 3D FE analysis of homogenized fibre-reinforced polymer (FRP) laminates, specifically relevant for pultruded quasi-orthotropic FRP components. The model's failure initiation assesses both in-plane and out-of-plane failure across the laminate's thickness. Subsequent failure progression involves reducing initial elastic and shear moduli, accounting for diverse damage directions, stress states, and establishing a constant residual stress post-limit strain.

Table 1. Mechanical properties of pGFRP I-section profile 152.4 × 76.2 × 6.35 (mm) obtained from coupon tests [8,18] and compressive strength from full-section tests [8,11].

Scale	Test method	Property	n	Zone	Average ± S.D.	Unit
Coupon [8], [18]	Compression: ASTM D6641 [26]	$f_{x,c}$	6	Web	437 ± 26	(MPa)
			6	Flange	448 ± 41	(MPa)
		$f_{y,c}$	6	Web	104 ± 11	(MPa)
		$E_{x,c}$	6	Web	24.6 ± 0.7	(GPa)
			6	Flange	26.3 ± 2.2	(GPa)
		$E_{y,c}$	6	Web	10.9 ± 1.3	(GPa)
		$\nu_{xy,c}$	9	Web	0.33 ± 0.05	( )
			6	Flange	0.34 ± 0.06	( )
	Tension: ISO-527-4 [27]	$f_{x,t}$	6	Web	426 ± 15	(MPa)
		$f_{y,t}$	6	Web	121 ± 9	(MPa)
		$E_{x,t}$	6	Web	28.8 ± 2.2	(GPa)
		$E_{y,t}$	6	Web	10.3 ± 0.5	(GPa)
	Shear in-plane: ASTM D5379 [28]	$f_{xy,v}$	6	Web	65 ± 2	(MPa)
		G_{xy}	6	Web	4.2 ± 0.6	(GPa)
Full-section [8], [11]	Compression: Non-standardized	$f_{x,c}$	15	Full-section	216 ± 23	(MPa)
		$E_{x,c}$	5	Full-section	29.8 ± 3.8	(GPa)

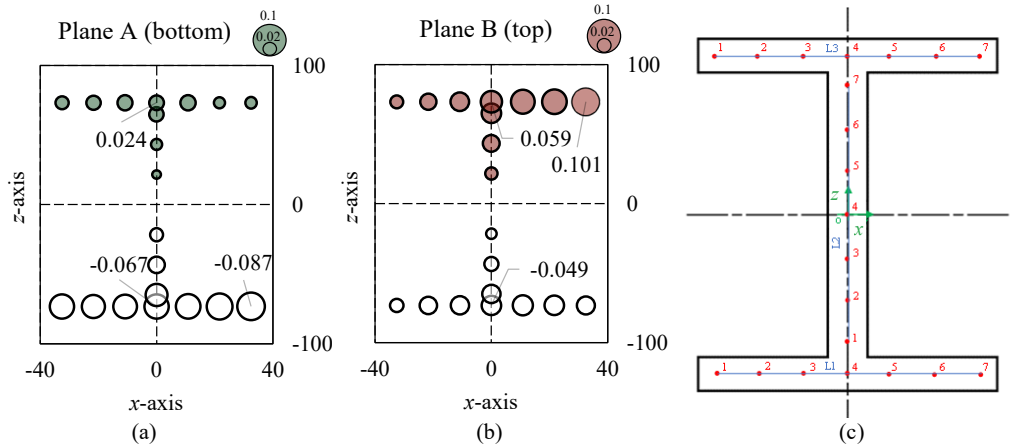

Figure 1. Experimental measurements of the out-of-plane (y-direction) end surface imperfections of an pGFRP I-section profile, indicating the non-planar surface in cut plane (a) A, (b) B and (c) point discretization.

With respect to the damage propagation model, it considers three main stages: (i) undamaged, (ii) damage progression and (iii) constant stress. The first stage is characterized by a linear elastic behaviour, with negligible influence of damage in the model. Subsequently, in the second stage, the elastic modulus starts to decrease, following an exponential damage law proposed by Matzenmiller *et al.* [23] (known as MLT model), which can reach a residual elastic modulus at the maximum damage allowed in this stage. After a certain limit strain is reached, the model is characterized by a constant stress (lower than the ultimate strength), which is defined here as the third stage. In order to avoid mesh dependency, a mesh regularization scheme was introduced between the second and third stages, comprising a smoothened linear transition (from damage progression to constant stress), following a similar procedure to that proposed by Bazant [29].

4 Simulations

4.1 Description of FE model

FE models were developed using the ABAQUS FE software package [16]. The stub column models comprise a pGFRP I-section profile I152×76×6.35 (mm) with rounded web-flange junction corner (corner radius equal the thickness value), with non-planar end surfaces (following the measurements of Figure 1) in contact with 30 mm thick rectangular flat steel plates, depicted in Figure 2.

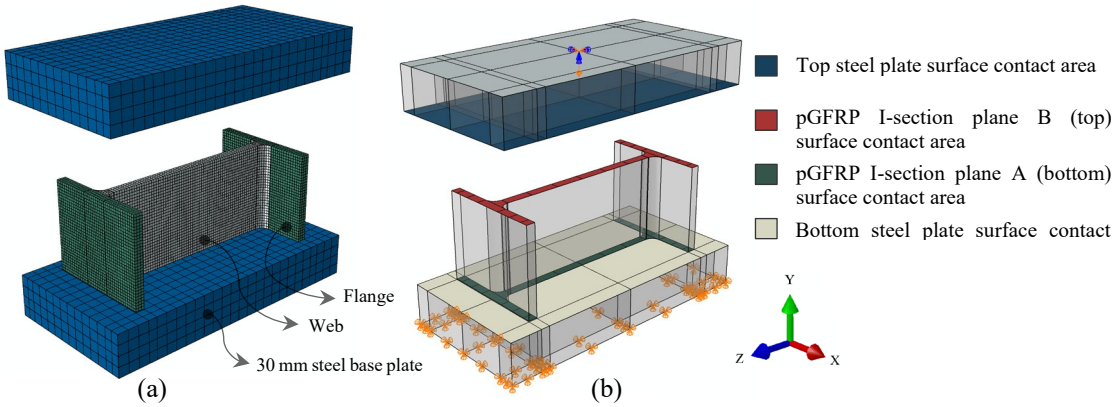

Figure 2. Finite element model of the stub column: (a) mesh discretization of each model part and (b) boundary condition and contact areas in the computational model (indicating plane A and plane B according to Figure 1).

Three materials were considered in the model (Figure 2(a)): steel for the base plates, with perfectly elastic behaviour (Es=200 GPa and v=0.3); and two pGFRP materials, one for the web and another one for the flange of the I-section profile. The rounded corner for the web-flange junction was considered with the same mechanical properties from the web. The orthotropic mechanical properties of the I-section profile considered as input were the ones obtained from the coupon tests reported in Table 1. The failure initiation and damage propagation model [14] (briefly described in section 3) were integrated into a user material (UMAT) subroutine, coded in Fortran 77 [30], with the input parameters calibrated in Costa *et al.* [25].

The element type used in the FE model is an 8-node linear brick C3D8R with reduced integration and enhanced hourglass control, with approximated element size control of 2 mm for the pGFRP I-section, resulting in at least three elements through the wall thickness, as illustrated in Figure 2(a).

The bottom surface of the bottom steel plate was considered clamped, and the top surface of the top plate was considered fixed in all degrees of freedom, except in the direction of the imposed displacement (Uy), where a displacement of 4 mm was imposed. The contact between the steel plates and the pGFRP profile end cut surfaces was modelled considering a tangential penalty behaviour with a constant friction coefficient of 0.3 and a normal behaviour simulated as “Hard contact”. Figure 2(b) indicates the contact areas and boundary conditions.

The nonlinear solver used Newton-Raphson incremental-iterative method considering the nonlinear effects of large deformations, with displacement control and auto stabilization active, assuming an initial increment of 10^{-3}, a minimum increment of 10^{-15} and a maximum increment of 10^{-1}.

4.2 Results and discussion

As mentioned, the computational FE modelling developed in this study aims to understand the impact of non-planar end surfaces, which are often generated during manufacturing, in the compressive response of full-section pGFRP profiles. To address this, three types of models are compared with different flatness of end surfaces: (i) perfectly flat, (ii) incorporating the experimentally measured values, as shown in Figure 1, and (iii) those results amplified by a factor of 5.4, simulating an error in parallelism of 0.5 mm, the acceptable limit according to ISO 23930:2023 [31]. The results of this analysis are depicted in Figure 3 in terms of load vs. shortening response and failure pattern.

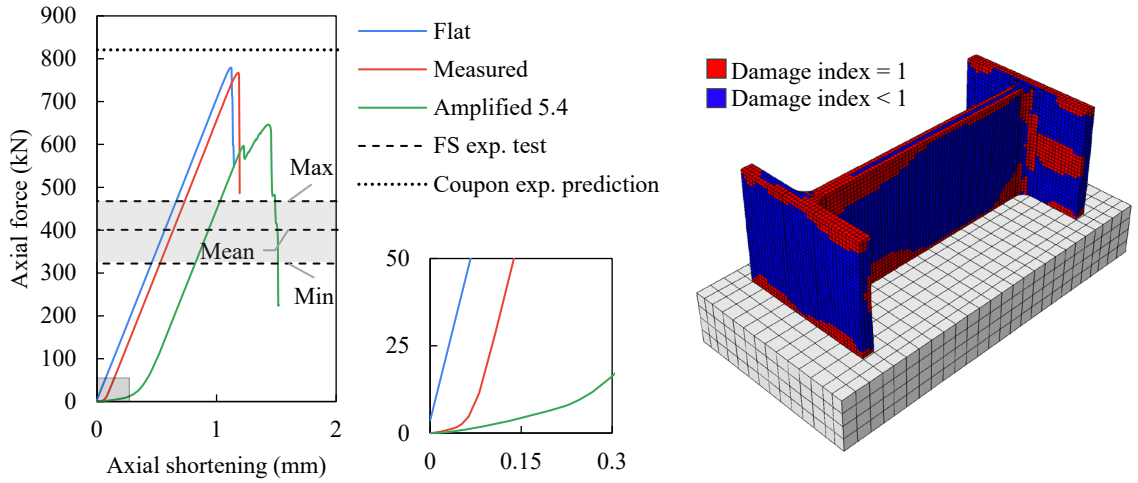

Figure 3. Finite element results for the pGFRP I-section stub column: (a) axial force *vs* axial shortening and (b) damage failure pattern of the experimental measured model at the ultimate load.

Figure 3(a) depicts the load *vs* axial shortening behaviour for the three FE models featuring different end surface conditions. One clear observation is that as the irregularities of the end surfaces are amplified, the compressive capacity of the stub column tends to decrease. Compared to the model with flat surface, the strength reduction is -1.6% and -17.1% for the model with the measured surface and the model with the amplified measured surface, respectively. This reduction can be due to localized crushing phenomena occurring in certain regions of the profile, resulting in premature structural failure. Furthermore, there is also an evident "toe effect" (as shown in the zoomed detail in Figure 3(a)) during the initial stages, which is more pronounced for higher defects. In contrast, the perfectly flat end surface exhibits no "toe effect," as expected, due to the uniform contact with the steel plates across the pGFRP cross-section during the initial loading stages. Figure 3(b) depicts the failure pattern for the model with imperfections as measured, at the ultimate load level. Failure occurs near the contact regions, in this case with more pronounced damage observed in one of the flanges (note that the geometry is not symmetric).

When comparing the computational results with the experimental data (compression tests in Table 1), the present models considerably overestimate the FS experimental ultimate loads, but also slightly underestimate the SSC test loads. Compared to the experimental FS tests, the computational strength prediction is 94%, 91%, and 61% higher for the models with flat surface, as-measured surface, and amplified end surface, respectively. On the other hand, they compare relatively well with the SSC tests prediction, with relative differences of -5%, -6.7%, and -21.3% for the models with flat surface, as-measured surface, and amplified end surface, respectively. These results indicate that the contribution to the differences between the predictions and the experimental FS results is relatively small. Thereafter, the differences between FE results and FS compressive tests are likely caused by factors (not considered in the FE models), such as (i) the reduction in strength and stiffness at the web-flange junctions, (ii) sudden changes in the orthotropic orientation at the interface between the web and flange, instead of a smooth transition (considering the rounded corners), which may impact the predictions, and (iii) coupling between delamination damage and longitudinal compression.

5 Conclusions

This study focused on understanding the initiation and progression of damage in pGFRP I-section stub columns under various end cutting surface conditions, while also considering the contact effect between steel base plates and the composite profiles. The computational model showed that these end cutting surfaces significantly impact the compressive capacity of the stub columns. Comparing the flat surface model with the amplified cutting surface model (defined as 5.4 times the as-measured model, in accordance with the limit defined in ISO 23930:2023), the FS compressive strength reduction was estimated to be 17%. These findings highlight the need to develop more accurate predictions of the crushing phenomenon in future design guidelines for pultruded profiles. In this context, it is imperative for current codes to account for this effect, ensuring that the crushing phenomenon is considered in its true value.

As part of future research, material characterization of the material in the out-of-plane direction under tension is planned to allow refining the damage model [14], including the integration of additional damage modes and the modelling of the radial orthotropic variation of material properties at the corner of the web-flange junction including the resin-rich core. Additionally, testing of slender pGFRP columns with different shapes and higher lengths is also planned to better understand the buckling-crushing interaction phenomenon. Subsequently, there are plans to develop design provisions to predict the ultimate capacity of pGFRP columns, including the definition of partial safety factors through reliability analysis.

Acknowledgements. The first author gratefully acknowledges the financial support given by FCT in the context of the PhD scholarship SFRH/BD/04925/2021.This work was supported by FCT, through IDMEC, under LAETA, project UIDB/50022/2020. This work was supported by FCT, through CERIS, project UIDB/04625/2020. All authors gratefully acknowledge the financial support given by FCT to project Reliable-FRP (project PTDC/ECI-EGC/3916/2021).

Authorship statement. The authors hereby confirm that they are the sole liable persons responsible for the authorship of this work, and that all material that has been herein included as part of the present paper is either the property (and authorship) of the authors or has the permission of the owners to be included here.

References

[1] National Research Council of Italy NRCI, CNR-DT 205/2007 - Advisory Committee on Technical Recommendations for Construction - Guide for the Design and Construction of Structures made of FRP Pultruded Elements. Rome, Italy, 2008.
[2] American Composites Manufacturers Association, Pre-Standard for Load and Resistance Factor Design (LRFD) of Pultruded Fiber Reinforced Polymer (FRP) Structures (Final). Arlington, USA: Structural Engineers Institute SEI-ASCE, 2010.
[3] CROW-CUR, Recommendation 96:2019 - Fibre Reinforced Polymers in Buildings & Civil Engineering Structures – Recommendation 96:2019. Gouda, The Netherlands, 2019.
[4] Standard of China Engineering Construction Standardization Association, T/CECS 692-2020 - Technical Specification for Structure of Pultruded Fiber Reinforced Polymer Composites (in Chinese). Beijing, China: China Construction Industry, 2020.
[5] European Committee for Standardization, "CEN/TS 19101:2022 - Design of fibre-polymer composite structures," Technical Specification. Technical Committee CEN/TC 250, Brussels, Belgium, Nov. 2022.
[6] American Society for Testing and Materials, ASTM D6641/D6641M – 09 - Standard Test Method for Compressive Properties of Polymer Matrix Composite Materials Using a Combined Loading Compression (CLC). West Conshohocken, Pennsylvania, United States: ASTM International, 2009. doi: 10.1520/D6641.
[7] European Standard, EN ISO 14126:2001 - Fibre-Reinforced Plastic Composites — Determination of Compressive Properties in the In-Plane Direction (version in Spanish). Bruxelles, 2001. Accessed: Jul. 30, 2022. [Online]. Available: https://www.iso.org/standard/23638.html
[8] J. C. Ramos, "Compressive Resistance of Pultruded GFRP Profiles," Master Dissertation in Civil Engineering (in Portuguese), Instituto Superior Técnico, University of Lisbon, Lisbon, Portugal, 2020.
[9] C. Wu, J. Tian, Y. Ding, and P. Feng, "Axial compression behavior of pultruded GFRP channel sections," Compos Struct, vol. 289, p. 115438, Jun. 2022, doi: 10.1016/J.COMPSTRUCT.2022.115438.
[10] J. A. De Lazzari, J. Gonilha, Nuno Silvestre, and J. R. Correia, "Quasi-static axial crushing behaviour of pultruded glass-fibre reinforced polymer profiles," in 6as Jornadas Portuguesas de Engenharia de Estruturas - JPEE, Carlos Pina, José Manuel Catarino, Ana Sofia Louro, and Teresa O. Santos, Eds., Lisboa: LNEC, 2022, pp. 627–641. Accessed: Apr. 26, 2023. [Online]. Available: http://jpee2022.lnec.pt/atas/atas.pdf

[11] J. A. Lazzari, J. Gonilha, N. Silvestre, and J. R. Correia, "Material crushing behaviour of pultruded GFRP stub columns: experimental study," in 11th International Conference on Fiber-Reinforced Polymer (FRP) Composites in Civil Engineering (CICE 2023), K. A. Harries, D. C. T. Cardoso, and F. A. Silva, Eds., Rio de Janeiro, Jun. 2023, pp. 1–12. doi: 10.5281/zenodo.8066292.
[12] G. J. Turvey and Y. Zhang, "Tearing failure of web–flange junctions in pultruded GRP profiles," Compos Part A Appl Sci Manuf, vol. 36, no. 2, pp. 309–317, Feb. 2005, doi: 10.1016/J.COMPOSITESA.2004.06.009.
[13] G. J. Turvey and Y. Zhang, "Shear failure strength of web–flange junctions in pultruded GRP WF profiles," Constr Build Mater, vol. 20, no. 1–2, pp. 81–89, Feb. 2006, doi: 10.1016/J.CONBUILDMAT.2005.06.045.
[14] J. Gonilha, N. Silvestre, J. R. Correia, V. Tita, and D. Martins, "Novel progressive failure model for quasi-orthotropic pultruded FRP structures: Formulation and calibration of parameters (Part I)," Compos Struct, vol. 255, p. 112974, Jan. 2021, doi: 10.1016/J.COMPSTRUCT.2020.112974.
[15] J. A. Lazzari, L. L. Martins, N. Silvestre, J. R. Correia, A. S. Ribeiro, and A. Pinheiro, "Characterization of 3D geometrical imperfections of pultruded GFRP profiles: introduction of a novel methodology," in 11th International Conference on Fiber-Reinforced Polymer (FRP) Composites in Civil Engineering (CICE 2023), K. A. Harries, D. C. T. Cardoso, and F. A. Silva, Eds., Rio de Janeiro, Jun. 2023. doi: 10.5281/zenodo.8066296.
[16] Dassault Systèmes Simulia Corp., "Abaqus/CAE 2018." Johnston, RI, USA, 2018.
[17] Creative Composites Group, "Creative Composites Group All Categories Catalogue," Jul. 18, 2022. https://catalog.creativecompositesgroup.com/viewitems/all-categories (accessed Jul. 18, 2022).
[18] L. Almeida-Fernandes, N. Silvestre, J. R. Correia, and M. Arruda, "Compressive transverse fracture behaviour of pultruded GFRP materials: Experimental study and numerical calibration," Compos Struct, vol. 247, no. February, 2020, doi: 10.1016/j.compstruct.2020.112453.
[19] S. Tsai, "Strength theories of filamentary structure," in Fundamental aspects of fiber reinforced plastic composites, R. Schwartz and H. Schwartz, Eds., New York: Wiley Interscience, 1966, pp. 3–11. Accessed: Aug. 31, 2023. [Online]. Available: https://cir.nii.ac.jp/crid/1572824500217112448
[20] S. W. Tsai and E. M. Wu, "A general theory of strength for anisotropic materials," J Compos Mater, vol. 5, no. 1, pp. 58–80, Jan. 1971, doi: 10.1177/002199837100500106.
[21] Z. Hashin, "Failure criteria for unidirectional fiber composites," J Appl Mech, vol. 47, no. June, pp. 329–334, 1980.
[22] I. Lapczyk and J. A. Hurtado, "Progressive damage modeling in fiber-reinforced materials," Compos Part A Appl Sci Manuf, vol. 38, no. 11, pp. 2333–2341, Nov. 2007, doi: 10.1016/j.compositesa.2007.01.017.
[23] A. Matzenmiller, J. Lubliner, and R. L. Taylor, "A constitutive model for anisotropic damage in fiber-composites," Mechanics of Materials, vol. 20, pp. 125–152, 1995, doi: 10.1016/0167-6636(94)00053-0.
[24] P. P. Camanho and C. G. Davila, "Mixed-Mode Decohesion Finite Elements for the Simulation of Delamination in Composite Materials: NASA/TM-2002-211737," Washington, DC, Jun. 2002. Accessed: Aug. 31, 2023. [Online]. Available: https://ntrs.nasa.gov/citations/20020053651
[25] D. Costa, J. A. Gonilha, and N. Silvestre, "Calibration and validation of a 3D homogenised model to simulate the damage progression of pultruded GFRP composites," Eng Fail Anal, vol. 149, p. 107261, Jul. 2023, doi: 10.1016/j.engfailanal.2023.107261.
[26] American Society for Testing and Materials, D6641/D6641M-14: Standard Test Method for Compressive Properties of Polymer Matrix Composite Materials Using a Combined Loading Compression (CLC) Test Fixture. 2014. doi: 10.1520/D6641_D6641M-14.
[27] International Organization for Standardization, ISO-527-4:1997 - Determination of Tensile Properties - Part 4: Test Conditions for Isotropic and Orthotropic Fiber-Reinforced Plastic Composites. Bruxelles, 1997.
[28] American Society for Testing and Materials, ASTM D5379/D5379M – 05 Standard: Standard Test Method for Shear Properties of Composite Materials by the V-Notched Beam Method. American Society for Testing and Materials, no. March 2005. 2005. doi: 10.1520/D5379_D5379M-05.
[29] Z. P. Bazant, "Imbricate continuum and progressive fracturing of concrete and geomaterials," Meccanica, vol. 19, no. S1, pp. 86–93, Mar. 1984, doi: 10.1007/BF01558458.
[30] SunSoft, "Fortran 77 4.0 User's Guide," no. 802-2997–10. Adobe PostScript, Moutain View, CA, pp. 1–422, 1995.
[31] International Organization for Standardization, ISO 23930 - Fibre Reinforced Plastic Composites – Full Section Compression Test for Pultruded Profiles. Geneva, Switzerland, 2023. Accessed: May 09, 2023. [Online]. Available: https://www.iso.org/standard/77390.html